Published in final edited form as:

Biochim Biophys Acta Mol Basis Dis. 2017 December ; 1863(12): 3277–3285. doi:10.1016/j.bbadis.2017.09.021.

Germline deletion of Krüppel-like factor 14 does not increase risk of diet induced metabolic syndrome in male C57BL/6 mice

Carmen A. Argmann[1,#], **Sara Violante**[1,#], **Tetyana Dodatko**[1], **Mariana P. Amaro**[1], **Jacob Hagen**[1], **Virginia L. Gillespie**[2], **Christoph Buettner**[3], **Eric E. Schadt**[1], **Sander M. Houten**[1]

[1]Department of Genetics and Genomic Sciences and Icahn Institute for Genomics and Multiscale Biology, Icahn School of Medicine at Mount Sinai, New York, New York, USA

[2]Center for Comparative Medicine and Surgery, Icahn School of Medicine at Mount Sinai, New York, NY

[3]Department of Medicine and Diabetes, Obesity, and Metabolism Institute, Icahn School of Medicine at Mount Sinai, New York, New York, USA

Abstract

Objective: The transcription factor Krüppel-like factor 14 (KLF14) has been associated with type 2 diabetes and high-density lipoprotein-cholesterol (HDL-C) through genome-wide association studies. The mechanistic underpinnings of KLF14's control of metabolic processes remain largely unknown. We studied the physiological roles of KLF14 in a knockout (KO) mouse model.

Methods: Male whole body *Klf14* KO mice were fed a chow or high fat diet (HFD) and diet induced phenotypes were analyzed. Additionally, tissue-specific expression of *Klf14* was determined using RT-PCR, RNA sequencing, immunoblotting and whole mount lacZ staining. Finally, the consequences of KLF14 loss-of-function were studied using RNA sequencing in tissues with relatively high *Klf14* expression levels.

Results: KLF14 loss-of-function did not affect HFD-induced weight gain or insulin resistance. Fasting plasma concentrations of glucose, insulin, cholesterol, HDL-C and ApoA-I were also comparable between $Klf14^{+/+}$ and $Klf14^{-/-}$ mice on chow and HFD. We found that in mice expression of *Klf14* was the highest in the anterior pituitary (adenohypophysis), lower but detectable in white adipose tissue and undetectable in liver. Loss of KLF14 function impacted on the pituitary transcriptome with extracellular matrix organization as the primary affected pathway and a predicted link to glucocorticoid receptor signaling.

Conclusions: Whole body loss of KLF14 function in male mice does not result in metabolic abnormalities as assessed under chow and HFD conditions. Mostly likely there is redundancy for the role of KLF14 in the mouse and a diverging function in humans.

Address for correspondence: Sander Houten, Department of Genetics and Genomic Sciences, Icahn School of Medicine at Mount Sinai, 1425 Madison Avenue, Box 1498, New York, NY 10029, USA. Phone: +1 212 659 9222, Fax: +1 212 659 5657, sander.houten@mssm.edu.

[#]Both authors contributed equally

Keywords

Krüppel-like factor; adenohypophysis; genome-wide association studies; mouse model

1. Introduction

Krüppel-like factors (KLFs) are transcription factors characterized by three highly conserved C2H2 zinc fingers that play roles in many different biological processes ranging from pluripotency to metabolism [1, 2]. KLF14 is a relatively recently discovered member of this family. It is encoded by an intronless gene and has monoallelic maternal expression in all studied tissues in both human and mouse [3]. The physiological roles KLF14 remain largely unknown.

Potential clues into KLF14's function came from genome-wide association studies (GWAS). Several studies associated susceptibility to type 2 diabetes with markers (rs4731702 and rs972283) close to *KLF14* [4, 5]. These variants only increased risk when carried on the maternal chromosome [4] and correlated with lower expression of *KLF14* in adipose tissue [4, 5]. The same variants associate with high-density lipoprotein-cholesterol (HDL-C) and triglycerides (TGs) [6–8], although the association with TGs is female-specific [8]. Follow-up studies revealed that the *KLF14* locus is an adipose trans-expression quantitative trait locus (eQTL) hotspot and that the expression of several of these trans-mediated genes was significantly associated with metabolic traits [9, 10]. The association of variation near *KLF14* with several metabolic traits has been replicated in several non-European populations such as African Americans [11, 12]. Some mechanistic insight was obtained by using intermediate quantitative glycemic traits and revealed that the *KLF14* risk allele was characterized by primary effects on insulin sensitivity [13].

Only a few studies have addressed the mechanistic underpinnings of KLF14's control on metabolic processes. Overexpression of KLF14 in Hepatoma carcinoma Hepa1–6 cells was shown to increase glucose uptake by stimulating the PI3K/Akt pathway [14]. KLF14 also increased expression of sphingosine kinase 1 in human and mouse endothelial cells [15]. Sphingosine kinase 1 is responsible for the generation of the signaling lipid sphingosine-1-phosphate, which is an important component of HDL and plays a role in cardiovascular protection [16]. Others have highlighted a role for KLF14 in macrophage inflammatory response impacting on atherosclerosis development [17]. KLF14 was also reported to induce ApoA-I expression in human and mouse hepatocytes offering a mechanistic explanation for the observed association with HDL-C [18]. Perhexiline was identified as a potential KLF14 activator that can increase HDL-C in several mouse models [18]. These mechanisms involve a multitude of pathways and tissues and have not been replicated so far. Here we investigated the metabolic consequences of loss of KLF14 function in mice.

2. Materials and methods

2.1 Mice

Sperm of *Klf14*$^{+/-}$ mice (C57BL/6N-*Klf14*$^{tm1.1(KOMP)Vlcg}$) was obtained from the KOMP repository (University of California, Davis). In the Velocigene KOMP project [19], a targeted deletion was created via homologous recombination using a ZEN-UB1 cassette containing a lacZ reporter and a loxP flanked selection marker (hUbCpro-neo-p(A)). The targeted allele in these mice was designated tm1. Mice that contained the tm1 allele were bred to Cre-expressing mice resulting in the removal of the beta-actin promoter and the Neomycin gene that it activated. The resulting mice carried the tm1.1 allele and were used for this study (Fig. 1).

Mice were genotyped using a PCR with 3 primers (Fig. 1); Reg-LacF (5'-ACTTGCTTTAAAAAACCTCCCACA-3'), GT2-F (5'-CATGGTGGAAAGCTCTGGTT-3') and GT2-R (5'-CGGTCTAATGACCCTGGAAA-3'). The WT allele was amplified by GT2-F and GT2-R yielding a PCR product of 186 basepairs while the tm1.1 allele was amplified by Reg-LacF and GT2-R yielding a PCR product of ~380 basepairs. In the tm1.1 allele, the complete *Klf14* open reading frame is deleted. The insertion of the ZEN-Ub1 Velocigene cassette created a deletion of 1035bp between positions 30,907,660–30,908,694 of chromosome 6 (Genome Build37). The LacZ reporter is inserted just downstream of the *Klf14* startcodon. The 3'-UTR of *Klf14* is largely intact with the recombination event 59 basepairs downstream of the amber stopcodon. Thus the LacZ reporter can be used as an in situ reporter to determine the gene expression profile of *Klf14* [20–22].

2.2 Phenotyping protocol

All animal experiments were approved by the IACUC of the Icahn School of Medicine at Mount Sinai and comply with the National Institutes of Health guide for the care and use of Laboratory animals (NIH Publications No. 8023, revised 1978). We used male mice only and the entire cohort was obtained by heterozygote breeding pairs. Mice were on chow until 8–9 weeks of age. At this time, mice in the high fat diet (HFD) groups were switched to the TD.06414 diet (Envigo), which contains 60% kcal from fat and is typically used for diet-induced obesity. EchoMRI was performed to determine body composition measurements of fat, lean, free water, and total water masses at 16 weeks of age. An intraperitoneal glucose tolerance test (IPGTT) was performed at 19 weeks of age for which the mice were fasted overnight and then injected with glucose. Mice on the chow diet received 2g glucose per kg body weight (2g/kg), whereas mice on the HFD received 1g/kg glucose. Mice were euthanized at 20–21 weeks of age after overnight food withdrawal. They were first anesthetized with pentobarbital (100mg/kg IP) and then exsanguinated via the vena cava inferior. Blood was collected for the preparation of EDTA plasma and organs were snap frozen in liquid nitrogen and stored at −80°C for future analyses.

2.3 Whole mount lacZ staining

Whole mount lacZ staining to identify KLF14 expressing tissues was performed as described [21]. Mice were euthanized using CO_2 asphyxiation and 30 seconds after

spontaneous breathing stopped, they were perfused with ice cold 4% paraformaldehyde in PBS (pH 8.0) via the left cardiac ventricle. After fixation, tissues of interest were dissected and collected in jars with ice cold PBS (pH 8.0). After an additional 30 minutes of fixing, tissues were washed with PBS and stained overnight in lacZ staining solution (PBS pH8.0 containing 2mM $MgCl_2$, 0.01% deoxycholic acid, 0.02% IGEPAL CA-630, 0.1% X-Gal in DMF, 5mM potassium ferrocyanide and 5mM potassium ferricyanide) at 4°C. After staining, the tissues were rinsed with PBS, postfixed overnight and subsequently cleared in 50% and then 70% glycerol in PBS.

2.4 Plasma chemistry

Plasma was used for the determination of glycerol (Sigma), TGs (Infinity, Thermo Scientific), total cholesterol (Infinity, Thermo Scientific), HDL-C (Crystal Chem) and insulin (Crystal Chem). Values for TGs were obtained after subtraction of free glycerol. Plasma ApoA-I was quantified using immunoblot. For this assay, 0.5μL of plasma was separated on a Bolt™ 4–12% Bis-Tris Plus Gel, blotted onto nitrocellulose and detected using an Apolipoprotein A1 polyclonal antibody (PA1–23059, Thermo Fisher Scientific). ApoA-I was quantified using IRDye 800CW secondary antibodies (LI-COR) and Image Studio Lite software (version 5.2, LI-COR). Equal loading was checked by Ponceau S staining. Fast Protein Liquid Chromatography (FPLC) of lipoproteins in pooled plasma samples for each cohort was performed by the Mouse Metabolic Phenotyping Center (MMPC) at Vanderbilt University School of Medicine. Corticosterone was determined using ELISA (Immuno-Biological Laboratories America; IB79175) and an EnSpire 2300 multimode plate reader (PerkinElmer).

2.5 RNA isolation, cDNA synthesis and quantitative PCR

RNA was isolated using QIAzol lysis reagent followed by purification using the RNeasy kit (Qiagen). Given the intronless nature of the *Klf14* gene, a DNase digestion was carried out during the RNA purification. cDNA synthesis was performed with the SuperScript IV first strand synthesis system (Thermo Fisher Scientific) using random hexamers as primers. qRT-PCR was performed using the ABI Prism 7900HT with Bio-rad iQ SYBR Green Mastermix. Data were analyzed using the Applied Biosystems SDS software. All samples were analyzed in duplicate and expression values were normalized against *Rplp0*. Primers sequences are provided in Table S1.

2.6 Immunoblotting

There are currently antibodies against 3 different KLF14 epitopes commercially available. Please note that multiple vendors offer apparently identical antibodies. We used PA5–23784 (Thermo Fisher), HPA044729 (Sigma-Aldrich) and TA341450 (Origene). All these antibodies are raised against human KLF14 epitopes (amino acids 254–283, 276–310 and 2–51, respectively) and only the epitope for PA5–23784 is 100% conserved between human and mouse KLF14. We tested the reactivity of these antibodies on overexpressed mouse KLF14. Mouse KLF14 was overexpressed in HEK-293 cells through transient transfection of a plasmid encoding Myc-DDK-tagged mouse *Klf14* (Origene, MR221172). Both PA5–23784 and HPA044729 were able to recognize mouse KLF14 in immunoblotting. Immunoblotting was performed as described (see 2.4).

2.7 RNA sequencing analysis

RNA samples were submitted to the Genomics Core Facility at the Icahn Institute and Department of Genetics and Genomic Sciences. cDNA libraries were prepared using the Illumina TruSeq RNA Library Preparation kit (#RS-122–2001). Samples were run on Illumina HiSeq 2500 at a read length of 100nt single end, and a depth of about 25 million per sample. Raw and processed data were returned, count files were generated by aligning the fastq files to the mouse genome mm10 (GRCm38.75) with STAR and counting overlaps with exons grouped at gene level by featureCounts [23].

Differential gene expression analysis was conducted with R packages limma (with voom transformation) [24] and DESeq2 [25]. Low count genes were removed in the limma analysis, genes were kept if they had at least one count per million in at least 4 samples. Cut off for differential expression was chosen at an adjusted p value (Benjamini, Hochberg) of <0.05.

2.8 Pathway enrichment analysis and transcription factor binding analysis

Pathway enrichment analysis was performed using the ClueGo v2.2.5 and CluePedia v1.2.5 plugins in Cytoscape (v. 3.4.0) with the GO, KEGG and Reactome databases (11/2016 download) [26, 27]. Cut off for pathway enrichment was chosen at an adjusted p value (Benjamini, Hochberg) of <0.05.

Iregulon v1.3 was used to create a gene regulatory network [28]. The following options *Motif collection*: 10K (9713 PWMs*), Putative regulatory region:* 10kb centered around TSS (10 species) alongside the program default settings for *Recovery* and *TF prediction* options were selected for the analysis.

2.9 Statistics

Data are displayed as the mean ± the standard deviation (SD) or standard error of the mean (SEM) as indicated in the figure legends. Differences between $Klf14^{+/+}$ and $Klf14^{-/-}$ mice were evaluated using a two-sided t-test, one-way analysis of variance with Bonferroni's multiple comparison test or a Kruskal-Wallis test with Dunn's multiple comparison post-tests as indicated (GraphPad Prism 6). Significance is indicated in the figures. Deviation of expected Mendelian segregation of genotypes was calculated with a X^2 test. Deviation of expected sex ratio of births was calculated with a binomial test.

3. Results

3.1 Characterization of *Klf14* KO mice

Mice with a targeted deletion of *Klf14* were created by the KOMP. We confirmed the correct targeting of *Klf14* using multiple assays. Genotyping results using PCR on genomic DNA were consistent with the VelociGene KOMP design (Fig. 1A). Sequencing of genomic DNA confirmed the correct insertion of the lacZ reporter in the *Klf14* locus. The $Klf14^{+/-}$ and $Klf14^{-/-}$ animals express lacZ instead of *Klf14* (see 3.3 and 3.4) and alignment of RNA sequencing reads is consistent with a deletion of the complete open reading frame in $Klf14^{-/-}$ animals (Fig. 1B).

Klf14$^{-/-}$ mice were generated through heterozygote breeding pairs. Segregation of genotypes was Mendelian (59 *Klf14*$^{+/+}$, 96 *Klf14*$^{+/-}$, 55 *Klf14*$^{-/-}$, X^2 not significant) with equal male-female ratio (98 male, 112 female; sex ratio of births is 88, binomial test not significant). Male and female *Klf14*$^{-/-}$ animals were fertile and appeared healthy.

3.2 Diet-induced obesity and associated metabolic phenotypes are not affected in male *Klf14* KO mice

Given KLF14's association with metabolic variables, we performed metabolic phenotyping of *Klf14*$^{+/+}$, *Klf14*$^{+/-}$ and *Klf14*$^{-/-}$ mice on chow and high fat diet (HFD). Feeding a HFD induced body weight gain, increased fat mass and caused glucose intolerance as measured by the IPGTT (Fig. 2A–C, Table 1). HFD feeding also increased the fasting plasma concentration of glucose, cholesterol, HDL-C and ApoA-I, but decreased TG levels. Unexpectedly, the loss of KLF14 function did not affect any of these diet-induced phenotypes (Fig. 2A–C, Table 1). *Klf14*$^{+/+}$ and *Klf14*$^{-/-}$ mice on chow and HFD did not differ in body weight, lean and fat body mass and fasting-induced body weight loss (Fig. 2A–C, Table 1). Glucose excursion during an IPGTT was also not different between *Klf14*$^{+/+}$ and *Klf14*$^{-/-}$ mice (Fig. 2A). Plasma clinical analytes indicative of metabolic health including concentrations of fasting glucose, insulin, TGs and cholesterol were also similar between *Klf14*$^{+/+}$ and *Klf14*$^{-/-}$ mice (Table 1).

The variation in body weight gain and fat mass was considerably larger in the *Klf14*$^{+/+}$ mice when compared to the *Klf14*$^{+/-}$ and *Klf14*$^{-/-}$ mice (Fig. 2B, C), but this could be explained by 2 low weight gainers in the *Klf14*$^{+/+}$ group. High phenotypic variation with low and high weight gainers in diet-induced obesity is typically observed in male C57BL/6 mice [29, 30]. The difference between the groups is smaller if we remove the 2 low weight gainers in the *Klf14*$^{+/+}$ group. Based on these observations, we conclude that loss of KLF14 function in male C57BL/6 mice does not affect diet-induced obesity phenotypes.

Liver-specific deletion of *Klf14* was recently shown to decrease HDL-C concentration. This effect was explained by the ability of KLF14 to modulate expression of ApoA-I [18]. However, in contrast to these reported findings, we did not observe changes in plasma lipoprotein profile, cholesterol, HDL-C and ApoA-I in *Klf14*$^{-/-}$ mice on chow or on HFD (Table 1, Fig. 2D, E). Consistently, expression of *Apoa1* in liver was not affected in *Klf14*$^{-/-}$ mice on HFD (Fig. 2F). Moreover, we were unable to reliably detect *Klf14* expression in liver (see 3.3).

3.3 *Klf14* is highly expressed in pituitary and testis and undetectable in liver

Previous work has shown that *Klf14* expression was higher in embryonic and extra-embryonic tissues when compared to expression in adult tissues and was undetectable in the adult liver [3]. The publicly available GeneAtlas data (BioGPS) and EST profiles (UniGene) further suggest that *Klf14* is highly expressed in mouse pituitary. Expression levels of *Klf14* are much lower in all other surveyed tissues. This observation is confirmed by other studies that profiled brain region-specific expression profiles and showed higher expression of *Klf14* in the pituitary compared to most other brain regions [31, 32]. To further study the expression profile of *Klf14* in the adult mouse, we surveyed cDNA of 12 different tissues by

PCR. *Klf14* expression was readily detectable in pituitary and several white adipose tissue (WAT) depots and was virtually undetectable in most other tissues including the liver and brown adipose tissue (BAT; Fig. 3A). In order to more accurately quantify and compare *Klf14* expression between different tissues, we performed RNA sequence analysis on RNA extracted from pituitary, inguinal WAT, gastrocnemius muscle, heart and liver tissues. While most sequencing reads mapping to *Klf14* were identified in pituitary, inguinal WAT also had significant *Klf14* expression (Fig. 3B). On the other hand, very low read counts were found in muscle and heart, and no *Klf14* mapped reads were identified in liver from two separate mouse cohorts (Fig. 3B). Unfortunately, we were unable to detect KLF14 protein in pituitary and liver (Fig. S1). KLF14 expression results could therefore not be further corroborated at the protein level.

Given the central role of the pituitary in neuroendocrine processes, we further studied the expression of *Klf14* in this tissue using whole mount lacZ staining. The pituitary is composed of two separate parts; the anterior pituitary or adenohypophysis (pars distalis and pars intermedia) and the posterior pituitary or neurohypophysis (pars nervosa). In order to visualize expression of *Klf14* in situ, we used the lacZ reporter that is expressed in $Klf14^{+/-}$ and $Klf14^{-/-}$ animals under control of the *Klf14* promoter. Pituitary displayed strong lacZ staining in the pars distalis and intermedia, indicating that the adenohypophysis is the major *Klf14* expressing tissue (Fig. 3C). Testis, epididymis and vas deferens were also positive for lacZ, which could indicate that *Klf14* is expressed in (developing) spermatozoa (Fig. 3D). Other tissues with lower levels of lacZ staining include gallbladder, muscle and several brain regions including hypothalamus and striatum (not shown). We observed no lacZ staining in liver, WAT and BAT. Overall our whole mount lacZ staining is consistent with pituitary being a primary *Klf14* expressing tissue in mouse.

Theoretically $Klf14^{+/-}$ animals should express one WT *Klf14* allele and one KO (lacZ) allele. However, we noted that some $Klf14^{+/-}$ animals were negative for lacZ staining. This is consistent with the reported imprinting at the *Klf14* locus in mouse oocytes [3]. To demonstrate the allele-specific expression at the *Klf14* locus in pituitary, we amplified the WT and KO allele on cDNA generated from adult $Klf14^{+/+}$, $Klf14^{+/-}$ and $Klf14^{-/-}$ animals. As expected, $Klf14^{+/+}$ and $Klf14^{-/-}$ animals expressed the *Klf14* or lacZ allele respectively, while the $Klf14^{+/-}$ animals expressed either the *Klf14* allele or the LacZ allele (Fig. 3E). Amplification on genomic DNA showed the presence of both alleles in these animals (Fig. 3E) indicating that *Klf14* is imprinted in adult mouse pituitary. Given the eQTL for *KLF14* in humans, we amplified the WT and KO allele on cDNA isolated from inguinal WAT of $Klf14^{+/-}$ animals on HFD and found that the $Klf14^{+/-}$ animals expressed lacZ or *Klf14* demonstrating that *Klf14* is also imprinted in adult adipose tissue (Fig. 3F).

3.4 Survey of tissue expression of *Klf14*

We surveyed frozen section lacZ staining of tissues of this *Klf14* KO mouse model, which are publicly available at the International Mouse Phenotyping Consortium website [20–22]. Pituitary was positive in pars distalis and pars intermedia confirming the results of the whole mount lacZ staining. Smooth muscle cell layers were lacZ positive in vasculature (e.g. in BAT and quadriceps muscle) and in the walls of the digestive system, urinary bladder and

seminal vesicles. There was also abundant lacZ staining in the male reproductive system with the smooth muscle cell layers, the apical cytoplasm of the epithelium in epididymis and the ciliated epithelium in the vas deferens being positive. The more mature layers of the seminiferous tubules in testis were also lacZ positive consistent with expression in (developing) spermatozoa. In addition, lacZ staining was also observed in the cartilage and chondrocytes of the trachea.

3.5 RNA sequencing reveals a role for KLF14 in pituitary function

In order to shed light on the physiological functions of KLF14 in mice, we performed RNA sequencing analysis of RNA isolated from inguinal WAT and pituitary of *Klf14*$^{+/+}$ and *Klf14*$^{-/-}$ animals on chow. Interestingly, we found no differentially expressed genes (DEGs) in the inguinal WAT samples when *Klf14*$^{+/+}$ mice were compared to *Klf14*$^{-/-}$ mice using DESeq2 or limma methods. Mouse genotyping errors and other sample process mishandling were excluded as the cause of the lack of DEGs as evidenced by Integrative Genomics Viewer analysis of *Klf14* reads and appropriate sample clustering in principal component analysis (data not shown). In contrast, we found 240 DEGs in pituitary of the same mice by DESeq2 (153 up and 87 down), of which 118 were detected also by limma methodology (Fig. 4A and Table S2). Expression of *Klf14* itself was most significantly altered with an almost ~2-fold upregulation suggesting the existence of a positive feed-back mechanism regulating pituitary *Klf14* expression levels. Q-PCR analysis of selected DEGs; *Cldn7*, *Rcn1*, *Megf10* and *Vwde,* validated the results obtained by RNA sequencing analysis (Fig. 4B).

Canonical pathway enrichment analysis of the 118 DEGs in pituitary revealed significant enrichment in pathways associated with extracellular matrix organization due to several collagen encoding genes, and neurotransmitter release cycle amongst other pathways (Fig. 4C and Table S3). Given that KLF14 is a transcription factor, we assessed whether the DEGs were enriched in KLF14 response elements, which would imply that they are direct KLF14 targets. We used the iRegulon plugin within cytoscape in order to identify ‘regulons’ using motif discovery in a set of co-regulated genes [28]. A regulon is defined as consisting of a transcription factor and its predicted direct transcriptional targets, which within their cis-regulatory control elements contain common transcription factor binding sites. The top transcription factor binding sites found enriched in the 118 DEGs was for elements related to KLF13 and KLF14 (Fig. 4D). Given the high degree of conservation of the C2H2 zinc fingers, it is not surprising to find multiple candidate KLF family members as potential binding transcription factors. Our results suggest that the genes with a KLF13/14 motif are potentially direct KLF14 targets in pituitary (Fig. 4E). The human orthologs of two DEGs (*Maged2* and *Slc35g2*) were also identified as having trans eQTLs at the *KLF14* locus [10], but this is not a significant overlap in a hypergeometric test. Of significance was the observation that *Nr3c1*, the glucocorticoid nuclear hormone receptor was not only significantly upregulated in the *Klf14*$^{-/-}$ mice, but also predicted to have both a KLF14 as well as an NR3C1 binding element (Fig. 4E). This suggests that KLF14 may impact the glucocorticoid signaling axis, but analysis of plasma corticosterone levels did not reveal differences between *Klf14*$^{+/+}$ and *Klf14*$^{-/-}$ animals (Table 1).

4. Discussion

We investigated the physiological functions of KLF14 by studying a whole body KO mouse model and focused on the metabolic role of this transcription factor by investigating insulin resistance and HDL-C in mice on chow and HFD. Our results indicate that KLF14 does not play a role in the development of diet-induced insulin resistance in male C57BL/6 mice. Moreover, our results do not support a major role of hepatic KLF14 in the regulation of ApoA-I and HDL-C levels, as was previously reported by others [18]. In fact, we found that expression of *Klf14* in mouse liver is virtually undetectable and that pituitary was the tissue with highest *Klf14* expression. RNA sequencing analysis of pituitary samples from $Klf14^{+/+}$ and $Klf14^{-/-}$ mice revealed that the loss of KLF14 function impacted on the pituitary transcriptome with extracellular matrix organization as the primary affected pathway. Analysis of transcription factor binding sites revealed a link to glucocorticoid receptor signaling.

Two reports describing the mechanism underlying the regulation of metabolic processes by KLF14 have focused on liver as the primary organ involved. Yang et al showed that *Klf14* mRNA and KLF14 protein expression is decreased in liver, adipose and muscle of C57BL/6 mice on HFD and db/db mice when compared to control animals [14]. In subsequent experiments the authors use ectopic KLF14 expression in the mouse hepatoma cell line Hepa1–6 and show that KLF14 stimulates insulin signaling via the classical PI3K/Akt pathway [14]. Consistent with these observations, Guo et al also showed that *Klf14* mRNA and KLF14 protein expression was significantly decreased in liver of C57BL/6 mice in response to a HFD and described similar results in ob/ob mice as well [18]. They showed that overexpression of human KLF14 in liver of mice that were fed a HFD, increased HDL-C, cholesterol efflux and ApoA-I expression. Conversely, they showed that liver-specific deletion of *Klf14* (floxed *Klf14* gene and *Alb*-Cre) decreased HDL-C and ApoA-I expression. The authors offered a mechanistic explanation by demonstrating that the ApoA-I promoter contained one KLF14-binding site. Moreover, perhexiline was identified as a KLF14 activator that raises HDL-C, ApoA-I and cholesterol efflux in vivo and reduced atherosclerosis development in $Apoe^{-/-}$ mice [18]. Our results do not support a role for KLF14 in hepatic ApoA-I production. The reason for this discrepancy is currently unclear, but may be caused by the use of different transgenic mouse models. Guo et al use a model with a floxed *Klf14* gene and *Alb*-Cre to delete *Klf14* in the liver. Expression of the *Alb*-Cre transgene is progressive with age, but can be detected in late fetal and neonatal stages of hepatocyte development [33]. The KOMP *Klf14* mouse model used in this study is a constitutive whole body KO, and its metabolic phenotype could therefore be compromised through early compensatory mechanisms. Regardless, we found no evidence for expression of *Klf14* in adult mouse liver as we were unable to amplify *Klf14* cDNA and did not find *Klf14* mapped reads in our liver RNA sequencing data. Surprisingly, both Yang et al [14] and Guo et al [18] report the use of male C57BL/6 mice similar to our studies. Moreover, the lack of expression of *Klf14* in liver in our RNA sequencing experiments does not appear to be mouse strain or institution specific because we analyzed two different mouse cohorts generated in different animal facilities: a second generation progeny of a cross between C57BL/6 and 129/P (B6129PF2) and second, a more advanced C57BL/6N backcross (4

generations [34]). Indeed, our data on the absence of *Klf14* expression in liver are consistent with previously published work [3] and publicly available data sources. We would also like to stress that assessing mRNA expression of *Klf14* by PCR requires DNase treatment of isolated RNA given the intronless nature of *Klf14*. Our well validated whole body *Klf14* KO mouse model did not display decreased ApoA-I mRNA nor did the animals have changes in plasma lipoprotein profile, cholesterol, HDL-C and ApoA-I, which can be viewed as consistent with the absence of expression of *Klf14* in the liver.

Both Yang et al [14] and Guo et al [18] show KLF14 expression in liver at the protein level, which is remarkable given the absence of *Klf14* mRNA in this tissue. The rabbit polyclonal antibody employed by Guo et al [18] (and possibly also by Yang et al [14]) is raised against the C-terminal region of human KLF14 (PA5–23784; amino acids 254–283) and is 100% conserved between human and mouse KLF14. By using the PA5–23784 and HPA044729 antibodies, we were able to detect overexpressed mouse KLF14. However, with both antibodies we were unable to detect a specific signal in whole pituitary extracts, nuclear pituitary extract and whole liver extracts (Fig. S1). Combined our data indicate that KLF14 expression in relatively low in pituitary and likely absent in liver.

Similar to mouse, human *KLF14* is expressed at higher levels in fetal tissue and placenta than in adult tissues and is absent in liver and lymphoblasts [3]. GTEx data confirm that overall expression of *KLF14* is low, but some expression is noted in testis, adrenal gland, spleen, visceral and subcutaneous adipose and breast (RPKM 1.6 and lower) [35]. Liver is the lowest *KLF14* expressing organ of all the 53 tissues in the GTEx dataset. Importantly GTEx identified cis eQTLs for the *KLF14* expressing tissues testis and subcutaneous adipose [35]. This supports the earlier GWAS studies that linked type 2 diabetes risk to a locus near *KLF14* that also harbors a cis eQTL in subcutaneous adipose [4, 5, 9, 10].

We failed to find significant consequences of KLF14 loss of function in mice on insulin resistance and adipose tissue gene expression. Male $Klf14^{-/-}$ animals on a C57BL/6 background had similar IPGTT, fasting insulin and fasting glucose when compared to $Klf14^{+/+}$ under chow and HFD conditions. Moreover, RNA sequencing analysis of inguinal WAT did not reveal differential expression between male $Klf14^{+/+}$ and $Klf14^{-/-}$ animals on a chow diet. There are several potential explanations for these observations. First, the metabolic phenotype could have been compensated for through developmental or other processes. Second, the effect of *Klf14* deletion on insulin resistance may be very small and thus our study could have been underpowered to detect such an effect. However, the numbers of animals that we used in our studies are not atypical for diet induced obesity studies in KO mouse models. We can therefore argue that any effect missed under these conditions is probably not biologically relevant. Alternatively, the regulation of adipose tissue gene expression by KLF14 may be more specific for humans and therefore not observed in mice. Indeed, there is some evidence that *KLF14* has been undergoing human-specific accelerated evolution [3]. Moreover, *KLF14* in humans does not appear to be highly expressed in pituitary (GTEx), indicating divergent roles between both species. Lastly, the function of KLF14 may be sex-specific and therefore not readily detectable in male mice. Indeed a conference abstract by Small et al suggests that the molecular cis and trans

regulatory effects are present in both sexes, but the cellular and whole body effects (type 2 diabetes, lipids, hip circumference) are female-specific [36].

Despite the lack of effect of *Klf14* deletion in adipose tissue, we did observe a significant effect on gene expression in the pituitary. Given the expression profile of *Klf14* in mouse pituitary, we anticipate that this is driven by changes in gene expression in the adenohypophysis. The DEGs were particularly enriched in KLF14 transcriptional binding motifs independently providing validity of the KO mouse model. We observed a previously uncharacterized link between KLF14 and glucocorticoid signaling through regulation of *Nr3c1* expression. This observation extends the known links between KLF4, KLF13 and KLF15 with glucocorticoid signaling [37–39]. Glucocorticoid signaling plays an important role in stress responses propagated by the HPA axis. We did not observe any signs of major HPA axis dysfunction such as changes in plasma corticosterone, glucose or insulin resistance. We speculate that perturbation of the HPA axis in $Klf14^{-/-}$ mice should be studied upon acute restraint stress. As the HPA axis is critical for metabolic control, our finding in mice may be relevant to explaining the GWAS links found in human adipose.

In summary, whole body loss of KLF14 function in the mouse did not result in metabolic abnormalities as assessed under chow or HFD conditions. Most likely there is redundancy for the role of KLF14 in the mouse and a divergent role for KLF14 in humans.

Supplementary Material

Refer to Web version on PubMed Central for supplementary material.

Acknowledgements

The authors thank Andrew Shin and Henry Ruiz of the Mount Sinai Diabetes, Obesity and Metabolism Institute for performing echoMRI analyses, Cindy Else and Ying Dai of the Comparative Pathology Laboratory for help with the whole mount lacZ staining, Carla Harris of the Vanderbilt Mouse Metabolic Phenotyping Center for performing the lipoprotein analyses, and Robin Sgueglia of the Biomarker Analytic Research Core at Albert Einstein College of Medicine for performing plasma corticosterone measurements. We acknowledge the help of the shared resource facilities at the Icahn School of Medicine at Mount Sinai (Colony Management, Real Time Polymerase Chain Reaction (qPCR), Mouse Genetics and Gene Targeting, Genomics Core and the Comparative Pathology Laboratory). This study was supported by grants to the Vanderbilt Mouse Metabolic Phenotyping Center (U24DK59637), the Diabetes Research Center (P60DK020541) and the ICTR Einstein-Montefiore (CTSA UL1TR001073).

Abbreviations

BAT	brown adipose tissue
DEG	differentially expressed genes
FPLC	Fast Protein Liquid Chromatography
GWAS	genome-wide association studies
HDL-C	high-density lipoprotein-cholesterol
HFD	high fat diet

IPGTT	intraperitoneal glucose tolerance test
KLF	Krüppel-like factors
KO	knockout
eQTL	expression quantitative trait locus
TG	triglyceride
WAT	white adipose tissue

References

[1]. Turner J, Crossley M, Mammalian Kruppel-like transcription factors: more than just a pretty finger, Trends Biochem Sci, 24 (1999) 236–240. [PubMed: 10366853]

[2]. Pearson R, Fleetwood J, Eaton S, Crossley M, Bao S, Kruppel-like transcription factors: a functional family, Int J Biochem Cell Biol, 40 (2008) 1996–2001. [PubMed: 17904406]

[3]. Parker-Katiraee L, Carson AR, Yamada T, Arnaud P, Feil R, Abu-Amero SN, et al. , Identification of the imprinted KLF14 transcription factor undergoing human-specific accelerated evolution, PLoS Genet, 3 (2007) e65. [PubMed: 17480121]

[4]. Kong A, Steinthorsdottir V, Masson G, Thorleifsson G, Sulem P, Besenbacher S, et al. , Parental origin of sequence variants associated with complex diseases, Nature, 462 (2009) 868–874. [PubMed: 20016592]

[5]. Voight BF, Scott LJ, Steinthorsdottir V, Morris AP, Dina C, Welch RP, et al. , Twelve type 2 diabetes susceptibility loci identified through large-scale association analysis, Nat Genet, 42 (2010) 579–589. [PubMed: 20581827]

[6]. Chasman DI, Pare G, Mora S, Hopewell JC, Peloso G, Clarke R, et al. , Forty-three loci associated with plasma lipoprotein size, concentration, and cholesterol content in genome-wide analysis, PLoS Genet, 5 (2009) e1000730. [PubMed: 19936222]

[7]. Global Lipids Genetics C, Willer CJ, Schmidt EM, Sengupta S, Peloso GM, Gustafsson S, et al. , Discovery and refinement of loci associated with lipid levels, Nat Genet, 45 (2013) 1274–1283. [PubMed: 24097068]

[8]. Teslovich TM, Musunuru K, Smith AV, Edmondson AC, Stylianou IM, Koseki M, et al. , Biological, clinical and population relevance of 95 loci for blood lipids, Nature, 466 (2010) 707–713. [PubMed: 20686565]

[9]. Small KS, Hedman AK, Grundberg E, Nica AC, Thorleifsson G, Kong A, et al. , Identification of an imprinted master trans regulator at the KLF14 locus related to multiple metabolic phenotypes, Nat Genet, 43 (2011) 561–564. [PubMed: 21572415]

[10]. Civelek M, Wu Y, Pan C, Raulerson CK, Ko A, He A, et al. , Genetic Regulation of Adipose Gene Expression and Cardio-Metabolic Traits, Am J Hum Genet, 100 (2017) 428–443. [PubMed: 28257690]

[11]. Chen G, Bentley A, Adeyemo A, Shriner D, Zhou J, Doumatey A, et al. , Genome-wide association study identifies novel loci association with fasting insulin and insulin resistance in African Americans, Hum Mol Genet, 21 (2012) 4530–4536. [PubMed: 22791750]

[12]. Ng MC, Saxena R, Li J, Palmer ND, Dimitrov L, Xu J, et al. , Transferability and fine mapping of type 2 diabetes loci in African Americans: the Candidate Gene Association Resource Plus Study, Diabetes, 62 (2013) 965–976. [PubMed: 23193183]

[13]. Dimas AS, Lagou V, Barker A, Knowles JW, Magi R, Hivert MF, et al. , Impact of type 2 diabetes susceptibility variants on quantitative glycemic traits reveals mechanistic heterogeneity, Diabetes, 63 (2014) 2158–2171. [PubMed: 24296717]

[14]. Yang M, Ren Y, Lin Z, Tang C, Jia Y, Lai Y, et al. , Kruppel-like factor 14 increases insulin sensitivity through activation of PI3K/Akt signal pathway, Cell Signal, 27 (2015) 2201–2208. [PubMed: 26226221]

[15]. de Assuncao TM, Lomberk G, Cao S, Yaqoob U, Mathison A, Simonetto DA, et al. , New role for Kruppel-like factor 14 as a transcriptional activator involved in the generation of signaling lipids, J Biol Chem, 289 (2014) 15798–15809. [PubMed: 24759103]

[16]. Sattler K, Levkau B, Sphingosine-1-phosphate as a mediator of high-density lipoprotein effects in cardiovascular protection, Cardiovasc Res, 82 (2009) 201–211. [PubMed: 19233866]

[17]. Wei X, Yang R, Wang C, Jian X, Li L, Liu H, et al. , A novel role for the Kruppel-like factor 14 on macrophage inflammatory response and atherosclerosis development, Cardiovasc Pathol, 27 (2017) 1–8. [PubMed: 27923151]

[18]. Guo Y, Fan Y, Zhang J, Lomberk GA, Zhou Z, Sun L, et al. , Perhexiline activates KLF14 and reduces atherosclerosis by modulating ApoA-I production, J Clin Invest, 125 (2015) 3819–3830. [PubMed: 26368306]

[19]. Skarnes WC, Rosen B, West AP, Koutsourakis M, Bushell W, Iyer V, et al. , A conditional knockout resource for the genome-wide study of mouse gene function, Nature, 474 (2011) 337–342. [PubMed: 21677750]

[20]. West DB, Pasumarthi RK, Baridon B, Djan E, Trainor A, Griffey SM, et al. , A lacZ reporter gene expression atlas for 313 adult KOMP mutant mouse lines, Genome Res, 25 (2015) 598–607. [PubMed: 25591789]

[21]. Tuck E, Estabel J, Oellrich A, Maguire AK, Adissu HA, Souter L, et al. , A gene expression resource generated by genome-wide lacZ profiling in the mouse, Dis Model Mech, 8 (2015) 1467–1478. [PubMed: 26398943]

[22]. Koscielny G, Yaikhom G, Iyer V, Meehan TF, Morgan H, Atienza-Herrero J, et al. , The International Mouse Phenotyping Consortium Web Portal, a unified point of access for knockout mice and related phenotyping data, Nucleic Acids Res, 42 (2014) D802–809. [PubMed: 24194600]

[23]. Dobin A, Davis CA, Schlesinger F, Drenkow J, Zaleski C, Jha S, et al. , STAR: ultrafast universal RNA-seq aligner, Bioinformatics, 29 (2013) 15–21. [PubMed: 23104886]

[24]. Smyth GK, limma: Linear Models for Microarray Data, in: Gentleman R, Carey VJ, Huber W, Irizarry RA, Dudoit S (Eds.) Bioinformatics and Computational Biology Solutions Using R and Bioconductor, Springer New York, New York, NY, 2005, pp. 397–420.

[25]. Love MI, Huber W, Anders S, Moderated estimation of fold change and dispersion for RNA-seq data with DESeq2, Genome Biol, 15 (2014) 550. [PubMed: 25516281]

[26]. Bindea G, Mlecnik B, Hackl H, Charoentong P, Tosolini M, Kirilovsky A, et al. , ClueGO: a Cytoscape plug-in to decipher functionally grouped gene ontology and pathway annotation networks, Bioinformatics, 25 (2009) 1091–1093. [PubMed: 19237447]

[27]. Bindea G, Galon J, Mlecnik B, CluePedia Cytoscape plugin: pathway insights using integrated experimental and in silico data, Bioinformatics, 29 (2013) 661–663. [PubMed: 23325622]

[28]. Janky R, Verfaillie A, Imrichova H, Van de Sande B, Standaert L, Christiaens V, et al. , iRegulon: from a gene list to a gene regulatory network using large motif and track collections, PLoS Comput Biol, 10 (2014) e1003731. [PubMed: 25058159]

[29]. Koza RA, Nikonova L, Hogan J, Rim JS, Mendoza T, Faulk C, et al. , Changes in gene expression foreshadow diet-induced obesity in genetically identical mice, PLoS Genet, 2 (2006) e81. [PubMed: 16733553]

[30]. Anunciado-Koza RP, Manuel J, Koza RA, Molecular correlates of fat mass expansion in C57BL/6J mice after short-term exposure to dietary fat, Ann N Y Acad Sci, 1363 (2016) 50–58. [PubMed: 26647164]

[31]. Kasukawa T, Masumoto KH, Nikaido I, Nagano M, Uno KD, Tsujino K, et al. , Quantitative expression profile of distinct functional regions in the adult mouse brain, PLoS One, 6 (2011) e23228. [PubMed: 21858037]

[32]. Hovatta I, Zapala MA, Broide RS, Schadt EE, Libiger O, Schork NJ, et al. , DNA variation and brain region-specific expression profiles exhibit different relationships between inbred mouse strains: implications for eQTL mapping studies, Genome Biol, 8 (2007) R25. [PubMed: 17324278]

[33]. Weisend CM, Kundert JA, Suvorova ES, Prigge JR, Schmidt EE, Cre activity in fetal albCre mouse hepatocytes: Utility for developmental studies, Genesis, 47 (2009) 789–792. [PubMed: 19830819]

[34]. Diekman EF, van Weeghel M, Wanders RJ, Visser G, Houten SM, Food withdrawal lowers energy expenditure and induces inactivity in long-chain fatty acid oxidation-deficient mouse models, FASEB J, 28 (2014) 2891–2900. [PubMed: 24648546]

[35]. GTEx-Consortium, Human genomics. The Genotype-Tissue Expression (GTEx) pilot analysis: multitissue gene regulation in humans, Science, 348 (2015) 648–660. [PubMed: 25954001]

[36]. Small K, Todorcevic M, Civelek M, El-Sayed Moustafa J, Mahajan A, Horikoshi M, et al., Adipose- and maternal- specific regulatory variants at KLF14 influence Type 2 Diabetes risk in women via a female-specific effect on adipocyte physiology and body composition, in: ASHG 2015 Annual Meeting, Baltimore, MD, 2015.

[37]. Shimizu N, Yoshikawa N, Ito N, Maruyama T, Suzuki Y, Takeda S, et al. , Crosstalk between glucocorticoid receptor and nutritional sensor mTOR in skeletal muscle, Cell Metab, 13 (2011) 170–182. [PubMed: 21284984]

[38]. Cruz-Topete D, He B, Xu X, Cidlowski JA, Kruppel-like Factor 13 Is a Major Mediator of Glucocorticoid Receptor Signaling in Cardiomyocytes and Protects These Cells from DNA Damage and Death, J Biol Chem, 291 (2016) 19374–19386. [PubMed: 27451392]

[39]. Sevilla LM, Latorre V, Carceller E, Boix J, Vodak D, Mills IG, Perez P, Glucocorticoid receptor and Klf4 co-regulate anti-inflammatory genes in keratinocytes, Mol Cell Endocrinol, 412 (2015) 281–289. [PubMed: 26001834]

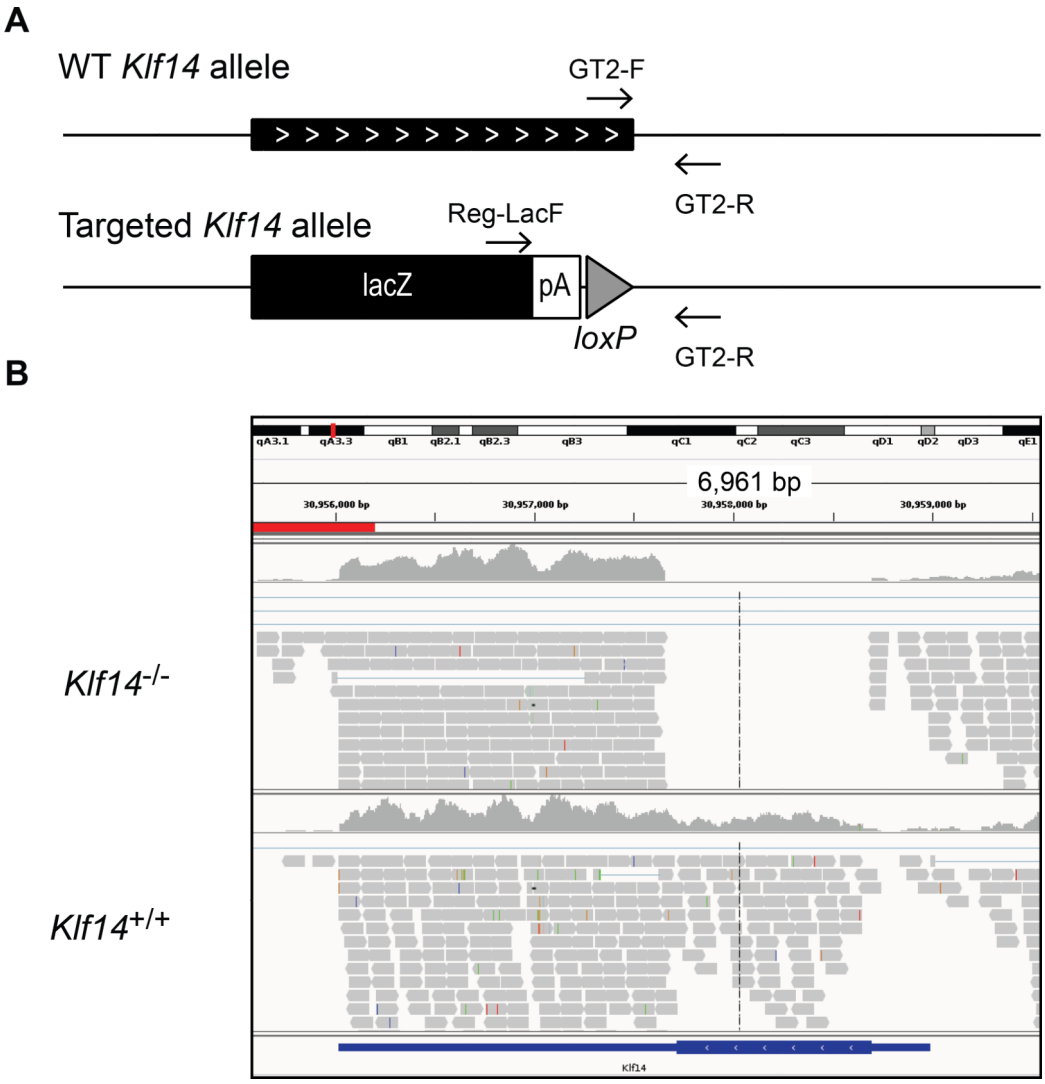

Figure 1.

The *Klf14* KO mouse. (A) Schematic representation of the WT and targeted *Klf14* allele. Primers used for genotyping are indicated. (B) Integrative Genomics Viewer representation of the aligned RNA sequencing reads at the *Klf14* locus in pituitary of a representative $Klf14^{+/+}$ and $Klf14^{-/-}$ sample.

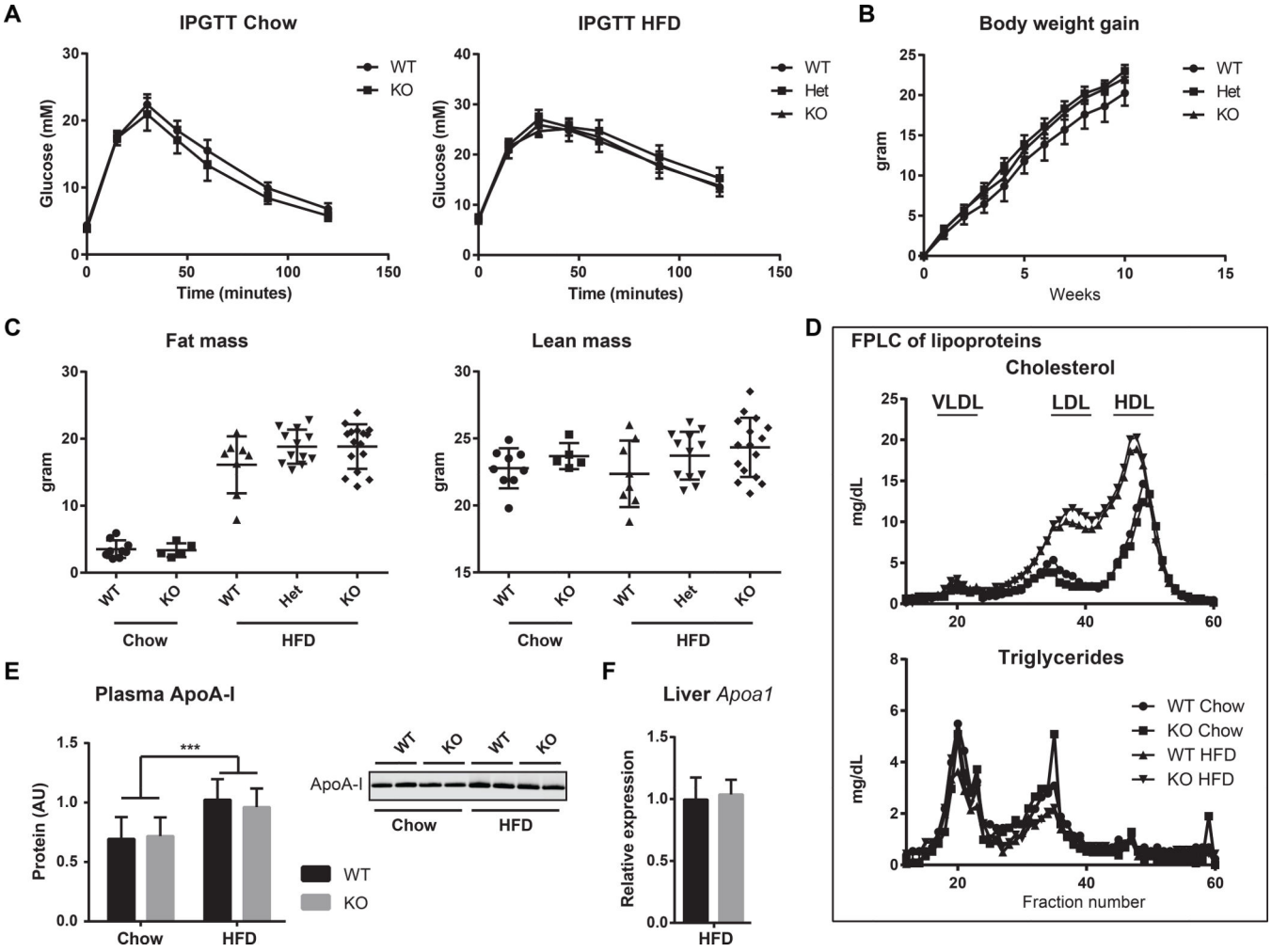

Figure 2.

Metabolic studies in the *Klf14* KO mouse. (A) IPGTT in mice on chow and HFD. Error bars in the IPGTT curves indicate SEM. (B) Weight gain of $Klf14^{+/+}$, $Klf14^{+/-}$ and $Klf14^{-/-}$ mice after switching to a HFD. Error bars indicate SEM. (C) Fat and lean mass as measured by EchoMRI in mice on chow and HFD. The scatter dot plots include mean and SD. (D) FPLC separation of a pooled plasma sample for each cohort. All fractions were assayed for cholesterol and triglycerides. The position of the lipoproteins is indicated in the chromatogram. (E) ApoA-I protein levels in plasma and one representative immunoblot of plasma ApoA-I protein. Error bars indicate SD, group size is 6, *** P< 0.001. (F) Expression of *Apoa1* normalized to 36B4 (*Rplp0*) in liver of $Klf14^{+/+}$ (n=4) and $Klf14^{-/-}$ (n=3) mice on HFD. Error bars indicate SD.

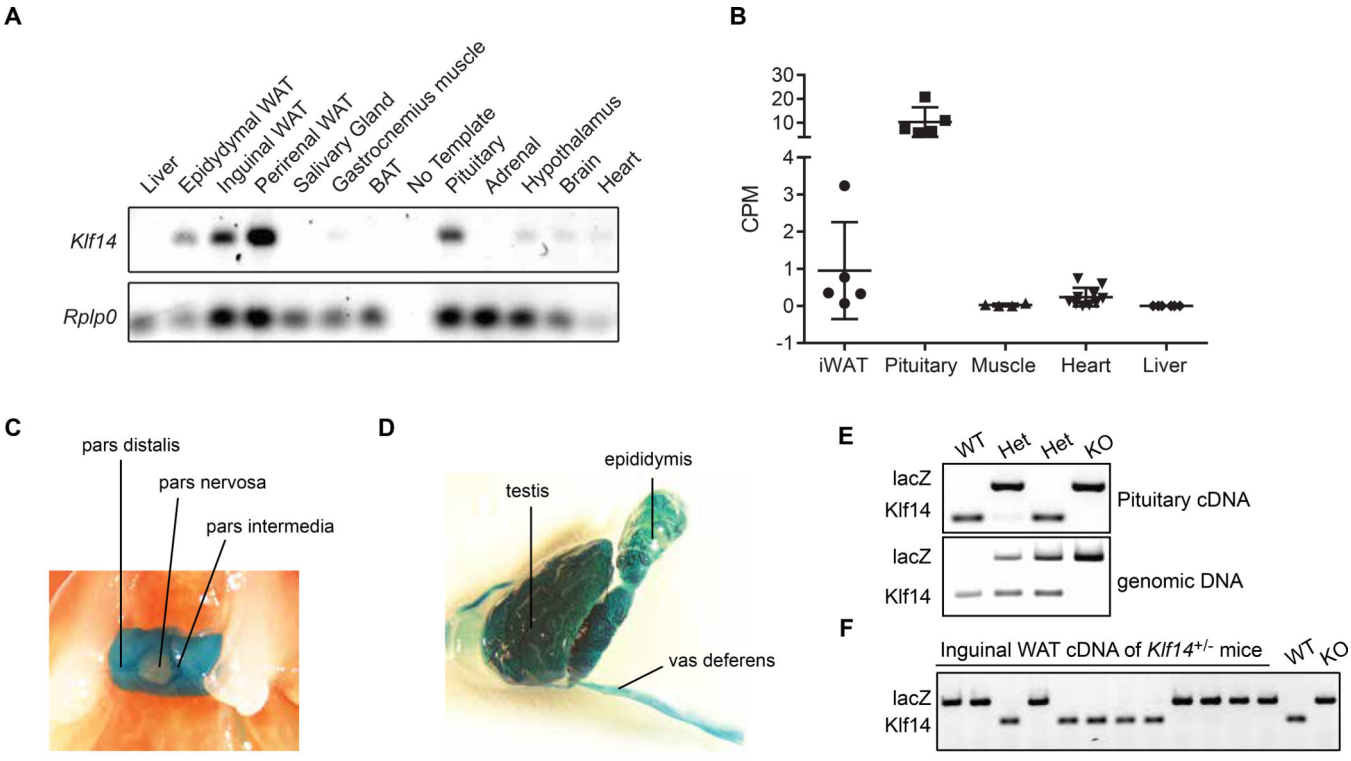

Figure 3.

Expression analysis of *Klf14* in the mouse. (A) Semi-quantitative analysis of *Klf14* expression across 12 mouse tissues. (B) Count per million mapped *Klf14* reads derived from RNA sequencing data from 5 different tissues. The scatter dot plots include mean and SD. (C) Whole mount LacZ staining of pituitary of a male $Klf14^{+/-}$ mouse. (D) Whole mount LacZ staining of testis, epididymis and vas deferens of a $Klf14^{-/-}$ mouse. (E) Allele-specific expression of *Klf14* in mouse pituitary. The *Klf14* and lacZ expressing alleles were amplified from pituitary cDNA and genomic DNA from the same animal. (F) Allele-specific expression of *Klf14* in inguinal WAT of $Klf14^{+/-}$ mice.

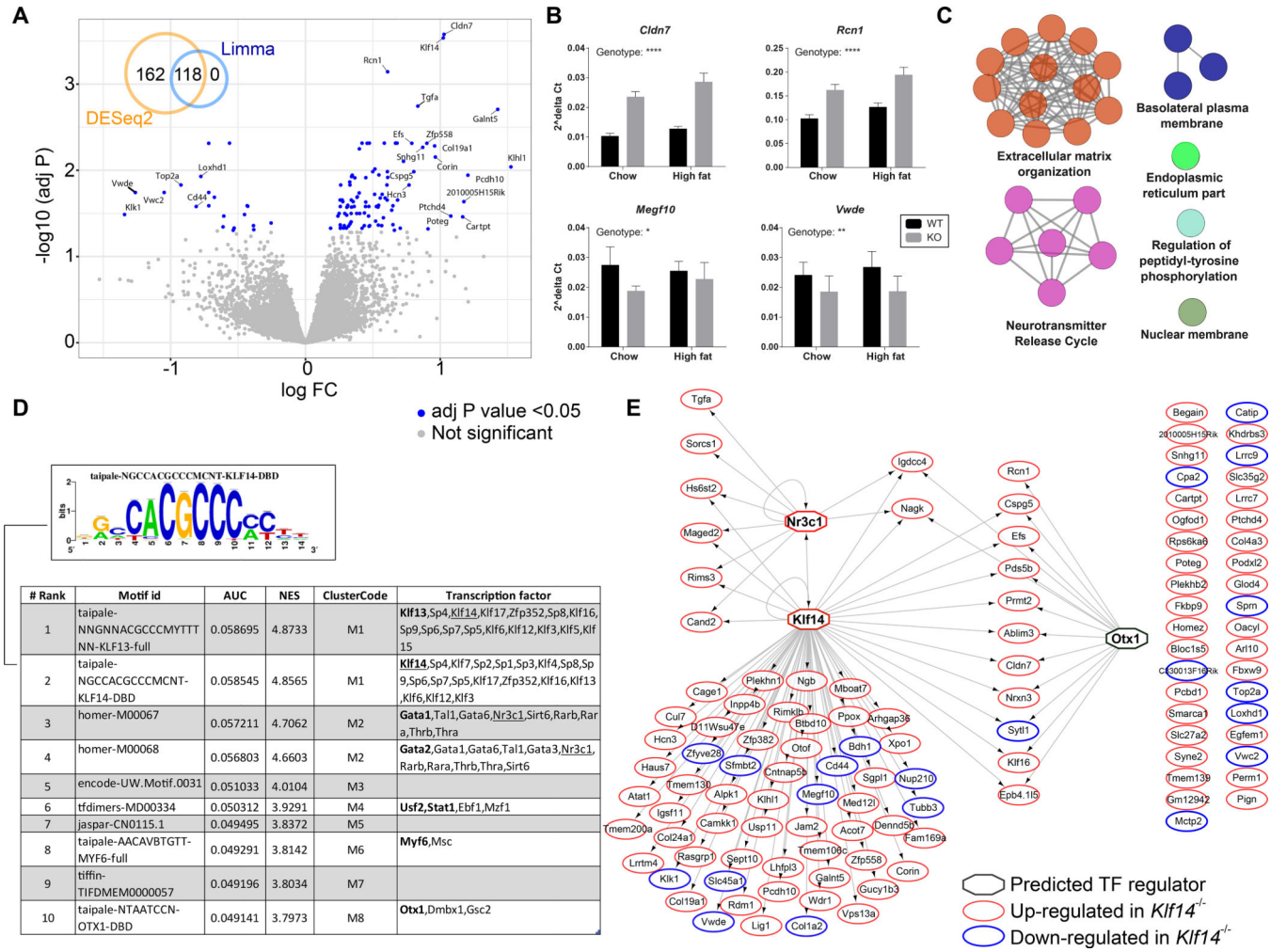

# Rank	Motif id	AUC	NES	ClusterCode	Transcription factor
1	taipale-NNGNNACGCCCMYTTTNN-KLF13-full	0.058695	4.8733	M1	**Klf13**,Sp4,Klf14,Klf17,Zfp352,Sp8,Klf16,Sp9,Sp6,Sp7,Sp5,Klf6,Klf12,Klf3,Klf5,Klf15
2	taipale-NGCCACGCCCMCNT-KLF14-DBD	0.058545	4.8565	M1	**Klf14**,Sp4,Klf7,Sp2,Sp1,Sp3,Klf4,Sp8,Sp9,Sp6,Sp7,Sp5,Klf17,Zfp352,Klf16,Klf13,Klf6,Klf12,Klf3
3	homer-M00067	0.057211	4.7062	M2	**Gata1**,Tal1,Gata6,Nr3c1,Sirt6,Rarb,Rara,Thrb,Thra
4	homer-M00068	0.056803	4.6603	M2	**Gata2**,Gata1,Gata6,Tal1,Gata3,Nr3c1,Rarb,Rara,Thrb,Thra,Sirt6
5	encode-UW.Motif.0031	0.051033	4.0104	M3	
6	tfdimers-MD00334	0.050312	3.9291	M4	**Usf2,Stat1**,Ebf1,Mzf1
7	jaspar-CN0115.1	0.049495	3.8372	M5	
8	taipale-AACAVBTGTT-MYF6-full	0.049291	3.8142	M6	**Myf6**,Msc
9	tiffin-TIFDMEM0000057	0.049196	3.8034	M7	
10	taipale-NTAATCCN-OTX1-DBD	0.049141	3.7973	M8	**Otx1**,Dmbx1,Gsc2

Figure 4.

RNA sequencing analysis of pituitary in the *Klf14* KO mouse. (A) Volcano plot displaying the log2 fold change versus -log10 of the adj P value for all genes in the comparison of *Klf14*$^{+/+}$ versus *Klf14*$^{-/-}$ in the pituitary of chow fed animals. The inset Venn diagram shows the overlap of genes detected as differentially expressed using either DESeq2 or limma packages. (B) qPCR validation of selected DEGs. Gene expression was calculated using the ΔCt method using *Rplp0* as the reference gene. All 4 genes were significantly altered in a two-way ANOVA. The significance for the variation in genotype is indicated in the figure; **** $P < 0.0001$, ** $P < 0.01$, and * $P < 0.05$. (C) A network displaying pathways significantly enriched for the 118 DEGs in pituitary. The color of the node represents the pathway term grouping. All nodes are significantly enriched at an adj P value <0.05. (D) A table summarizing the results of the Iregulon analysis, which lists the top transcription binding motifs and their associated transcription factors found enriched in the cis-regulatory regions of the 118 DEGs. The underlined TFs are the more likely candidates based on the input data. (E) A network representing the predicted targets (as oval nodes) of the top potential transcriptional regulators (as octagonal nodes). The color of the oval nodes

indicates whether that gene was up- or down-regulated in the pituitary of *Klf14*$^{-/-}$ mice when compared to *Klf14*$^{+/+}$ mice.

Table 1.

Analyzed variables in WT and *Klf14* KO mice on chow and high fat diet.

	KW	Chow diet		post	High fat diet			post
	Sig.	*Klf14* $^{+/+}$	*Klf14* $^{-/-}$	Sig.	*Klf14* $^{+/+}$	*Klf14* $^{+/-}$	*Klf14* $^{-/-}$	Sig.
Body weight (g)	****	27.7 ± 1.9	28.6 ± 1.4	#	40.8 ± 6.8	45.0 ± 3.5	45.4 ± 3.1	#
Lean mass (g)	#	22.8 ± 1.5	23.7 ± 1.0		22.4 ± 2.5	23.7 ± 1.8	24.3 ± 2.2	
Fat mass (g)	****	3.5 ± 1.3	3.4 ± 1.0	#	16.1 ± 4.3	18.8 ± 2.5	18.8 ± 3.3	#
Fasting-induced BW loss (g)	#	3.1 ± 0.4	2.9 ± 0.7		2.3 ± 0.5	2.7 ± 0.6	2.7 ± 0.5	
AUC BW gain (g * week)	#	ND	ND		111 ± 37	130 ± 27	125 ± 25	
Glucose (mmol/L)	**	5.0 ± 0.9	4.9 ± 0.5	#	7.6 ± 1.7	6.9 ± 1.9	6.7 ± 1.6	#
Insulin (ng/mL)	#	1.3 ± 0.8	1.3 ± 0.5		1.2 ± 0.3	1.1 ± 0.3	0.9 ± 0.2	
Triglycerides (mmol/L)	***	0.48 ± 0.14	0.42 ± 0.26	#	0.28 ± 0.06	0.22 ± 0.06	0.25 ± 0.11	#
Glycerol (mmol/L)	#	0.36 ± 0.08	0.31 ± 0.08		0.34 ± 0.05	0.35 ± 0.05	0.37 ± 0.07	
Cholesterol (mmol/L)	****	1.6 ± 0.2	1.5 ± 0.2	#	3.2 ± 0.8	3.2 ± 0.9	3.4 ± 0.7	#
HDL (mmol/L)	****	1.3 ± 0.2	1.2 ± 0.1	#	2.1 ± 0.3	2.1 ± 0.5	2.1 ± 0.4	#
ApoA-I (relative)	**	0.7 ± 0.2	0.7 ± 0.2	#	1.0 ± 0.2	ND	1.0 ± 0.2	#
Corticosterone (ng/mL)	#	179 ± 72	189 ± 74		229 ± 44	ND	221 ± 93	
AUC IPGTT (dose 2g/kg; mmol/L * minute)	#	1132 ± 355	1039 ± 372		ND	ND	ND	
AUC IPGTT (dose 1g/kg; mmol/L * minute)	#	ND	ND		1510 ± 449	1673 ± 587	1572 ± 364	
Heart weight (mg)	#	126 ± 17	124 ± 12		111 ± 10	121 ± 17	124 ± 17	
Liver weight (g)	**	1.12 ± 0.12	1.16 ± 0.22	#	1.47 ± 0.61	1.70 ± 0.51	1.66 ± 0.44	#

Values are the average ± SD. The values are sampled the following cohorts: Chow diet, 11 *Klf14*$^{+/+}$ and 6 *Klf14*$^{-/-}$; High fat diet, 8 *Klf14*$^{+/+}$, 11 *Klf14*$^{+/-}$ and 15 *Klf14*$^{-/-}$. Statistical analysis of the data was performed using a nonparametric Kruskal-Wallis (KW) test with Dunn's multiple comparison post tests for WT versus KO. AUC stands for area under the baseline corrected curve. Significance (Sig.) is indicated as follows

= not significant

* < 0.05

** < 0.01

*** < 0.001 and

**** < 0.0001. ND denotes not done.